PLOS ONE

RESEARCH ARTICLE

Synthesis, characterization, quantum chemical calculations and anticancer activity of a Schiff base *NNOO* chelate ligand and Pd(II) complex

Nizam Ahmad[1]*, El Hassane Anouar[2]*, Amalina Mohd Tajuddin[1,3], Kalavathy Ramasamy[4,5], Bohari M. Yamin[6], Hadariah Bahron[1]

1 Faculty of Applied Sciences, Universiti Teknologi MARA, Shah Alam, Selangor, Malaysia, **2** Department of Chemistry, College of Science and Humanities in Al-Kharj, Prince Sattam bin Abdulaziz University, Al-Kharj, Saudi Arabia, **3** Atta-ur-Rahman Institute for Natural Product Discovery, Bandar Puncak Alam, Selangor, Malaysia, **4** Faculty of Pharmacy, Universiti Teknologi MARA, Shah Alam, Selangor, Malaysia, **5** Collaborative Drug Discovery Research (CDDR) Group, Pharmaceutical and Life Sciences Community of Research, Universiti Teknologi MARA (UiTM), Shah Alam, Selangor, Malaysia, **6** Publication Enhancement Unit, Penerbit UKM, Universiti Kebangsaan Malaysia, Bangi, Selangor, Malaysia

* shahrulnizam85@gmail.com (NA); anouarelhassane@yahoo.fr (EHA)

Citation: Ahmad N, Anouar EH, Tajuddin AM, Ramasamy K, Yamin BM, Bahron H (2020) Synthesis, characterization, quantum chemical calculations and anticancer activity of a Schiff base *NNOO* chelate ligand and Pd(II) complex. PLoS ONE 15(4): e0231147. https://doi.org/10.1371/journal.pone.0231147

Editor: Mohammad Shahid, Aligarh Muslim University, INDIA

Received: September 27, 2019

Accepted: March 17, 2020

Published: April 14, 2020

Data Availability Statement: All relevant data are within the paper and its Supporting Information files.

Funding: The author received funding from research funding (600-IRMI/5/3 LESTARI (024/2019)) and the Ministry of Higher Education of Malaysia for SLAB/SLAI scholarship.

Competing interests: The authors have declared that no competing interests exist.

Abstract

This paper reports the synthesis, characterization, anticancer screening and quantum chemical calculation of a tetradentate Schiff base 2,2'-((1*E*,1'*E*)-((2,2-dimethylpropane-1,3-diyl)bis(azanylylidene))bis(methanylylidene))bis(4-fluorophenol) (**L2F**) and its Pd (II) complex (**PdL2F**). The compounds were characterized *via* UV-Visible, NMR, IR spectroscopy and single crystal x-ray diffraction. Density Functional Theory (DFT) and time-dependent DFT calculations in gas and solvent phases were carried out using B3LYP, B3P86, CAM-B3LYP and PBE0 hybrid functionals combined with LanL2DZ basis set. Complexation of **L2F** to form **PdL2F** was observed to cause a bathochromic shift of the maximum absorption bands of n–π* from 327 to 410 nm; an upfield shift for δ (HC = N) from 8.30 to 7.96 ppm and a decreased wavenumber for ν(C = N) from 1637 to 1616 cm^{-1}. Overall, the UV-Vis, NMR and IR spectral data are relatively well reproduced through DFT and TD-DFT methods. **L2F** and **PdL2F** showed IC_{50} of 90.00 and 4.10 μg/mL, respectively, against human colorectal carcinoma (HCT116) cell lines, signifying increased anticancer activity upon complexation with Pd (II).

Introduction

Schiff bases, also known as imines (C = N) or azomethines (HC = N) were first reported by Hugo (Ugo) Schiff (1834–1915) in 1864 [1]. They are commonly formed through the condensation reaction of primary amines with aldehydes or less commonly, ketones [2]. The resultant imines ($R_1HC = N–R_2$ or $R_1R_2C = N–R_3$), where R_1, R_2 and R_3 can be any aryl or alkyl groups, can form complexes with metal ions through donation of the lone pair of electrons of nitrogen. One of the most regularly reported *NNOO* ligands are the salen-type ligands, formerly termed

for a family of bisimine compounds, N, N′-bis (salicylidine) ethylenediamine derived from salicylaldehyde and ethylenediamine in 2:1 molar ratio [3]. In evolution, the family of the salen-type compounds is not only limited to ligands derived from ethylenediamine but also used to describe ligands derived from other primary diamines such as propanediamine and phenylenediamine. The products of the former are also known as salpn-type ligands and the latter are denoted as salophen-type ligands. This paper focuses on the former type of salen and its corresponding palladium (II) complex.

Schiff base ligands have become progressively popular in coordination chemistry owing to their capability to coordinate with many transition metals, stabilizing them in multiple oxidation numbers. This exceptional chelating ability is mainly empowered by the presence of azomethine nitrogen that carries a lone pair of electrons situated in an sp^2 hybrid orbital [4]. The effectiveness of Schiff bases as chelating agents is enhanced with the presence of O-H or S-H functional group(s) within 2–3 atomic distances from the azomethine group [5,6]. The stability of Schiff base complexes is largely enhanced through the chelate effect of the polydentate ligands.

Schiff bases are known for their wide potential as bioactive agents such as anticancer [7], antifungal [8,9] and antileishmanial [10]. Previously, we reported the structure-antioxidant activity relationship of a series of phenolic Schiff bases as free radical scavengers using both experimental and DFT calculations [11]. The complexation of Schiff bases as privileged ligands with metals increases their applicability in both chemical and biological processes [12]. Recently, we investigated the bioactivity of an N,O bidentate Schiff base, (E)-(4-methoxybenzylimino)methyl)phenol and its Ni(II) and Pd(II) complexes against HCT116 colorectal cancer cells and Escherichia coli, and the obtained results displayed that the parent ligand is a more superior anticancer and antibacterial agent than positive control [13].

Quantum chemical calculations are considered powerful tools to verify spectral data including the prediction of ^{1}H and ^{13}C NMR chemical shifts [14–16], UV-Visible absorption bands [17–19] and X-ray structure parameters [20, 21]. Reported studies proved that to predict the excited states of some natural compounds, the use of B3LYP and PBE0 hybrid functionals are appropriate to estimate the excited state energies [22–26]. Previously, we used B3P86 and B3LYP hybrid functionals to predict the maximum absorption bands of a series of natural polyphenols [27]. Lumpi et al. (2013) showed that the M06-2X hybrid functional was suitable to predict the absorption and emission spectra of oligothiophene-based compounds [28]. Quartarolo and Russo applied PBE0 and ab initio multi-reference coupled cluster with the resolution of identity approximation (RICC2) approaches to predict the UV-Visible spectra of pyranoanthocyanins, a class of derived anthocyanin molecules; they showed that the use of larger basis sets results in little improvement of excitation energies, and that the conformational effect has a slight influence on the λMAX predictions [29]. In another study, Sousa et al. (2012) tested B3LYP and PBE0, and long-range corrected ωB97X and ωB97XD hybrid functional to predict the absorption electronic spectra of the isopentaphyrin derivative and its lutetium complex; and they showed that ωB97XD is the most reliable to reproduce the absorption electronic spectra of the isopentaphyrin derivative and its lutetium complex [30]. In regard to the ^{1}H and ^{13}C chemical shift calculations, the gauge-independent atomic orbital (GIAO) method is one of the most common approaches used to predict nuclear magnetic shielding tensors (σiso) [31, 32].

The present study aims at investigating anticancer activity of a synthesized Schiff base L2F and its palladium (II) complex PdL2F. The ligand and its complex were characterized by single crystal x-ray diffraction, NMR, IR and UV-Vis spectroscopic techniques. To support the experimental data, DFT and TD-DFT calculations in gas and solvent phases were carried out to predict maximum absorption bands, vibrations modes and chemical shifts of L2F and PdL2F. In addition, the chelation effect of L2F on the experimental data is emphasized.

Material and methods

Starting materials and instruments

All chemicals and solvents purchased from commercial suppliers were used without further purification. The elemental analysis (C, H, and N) of ligand, L2F and complex, PdL2F were obtained from Thermo Scientific Flash 2000 Elemental Analyser. Melting points were determined using Stuart SMP10. Perkin-Elmer Spectrum One FTIR spectrometer using KBr pellets recorded infrared spectra of ligand, L2F and complex, PdL2F between 450–4000 cm^{-1}. ^{1}H and ^{13}C NMR spectra were recorded on a Bruker Varian 600 MHz spectrometer as $CDCl_3$ or DMSO-d6 solutions.

X-ray single crystal data for the coordination polymers were collected at 293(2) and 171(1) K on Bruker D8 QUEST with photon CCD area-detector diffractometer Mo-Kα (λ = 0.71073 Å). High-quality crystals were chosen using a polarizing microscope and mounted on a glass fibre. Data processing and absorption correction was performed using a multi-scan method. The structures were solved by direct method using SHELXS. All data were refined by full matrix least-squares refinement against |F2| using SHELXL [33], and the final refinement include atomic position for all the atoms, anisotropic thermal parameters for all the non-hydrogen atoms, and isotropic thermal parameters for the hydrogen atoms. The programs PLATON and Mercury were used throughout the study [34].

Synthesis

Synthesis of Schiff base L2F. **L2F** was prepared by adding a 10-mL hot ethanolic solution of DMPD (1 mmol, 0.1022 g) into a stirred equivolume ethanolic solution of 5-fluorosalicylaldehyde (2 mmol, 0.2802 g) (Fig 1). The solution was refluxed over a period of 4 h, cooled to room temperature and chilled overnight. The yellow precipitate obtained was filtered off, washed with cold EtOH and air-dried. The yellow single crystal of the compound was obtained upon slow evaporation from ethanol. The synthesized compound was identified as 2,2'-((1*E*,1'*E*)-((2,2-dimethylpropane-1,3-diyl)bis(azanylylidene))bis(methanylylidene))bis(4-fluorophenol), a tetradentate Schiff base assigned as L2F. Yellow solid; yield, 85.0%; m.p. 115–116 ˚C. Elemental analysis for L2F, analysed as $C_{19}H_{20}F_2N_2O_2$ (326.28 $gmol^{-1}$); % Found (Calc.) C, 65.81 (65.88): H, 5.80 (5.82); N, 8.23 (8.09); UV-Vis bands (MeCN, nm): π-π* (C = N) 257, n-π* (C = N) 327; IR bands (KBr pellet, cm^{-1}): ν(O-H) 3271, ν(C = N) 1637, ν(C-O) 1071, ν(C = C) 1583, ν(C-H sp^2) 3071, ν(C-H sp^3) 2956; ^{1}H NMR (500 MHz, $CDCl_3$, ppm): δ(OH) 13.25 (s, 1H), δ(HC = N) 8.30 (s, 1H); ^{13}C NMR (500 MHz, $CDCl_3$, ppm): δ(C-OH) 157.74, δ(C = N) 164.74.

Synthesis of complex PdL2F. **PdL2F** was synthesized by dissolving palladium (II) acetate (1 mmol, 0.2248 g) in 20 mL of acetonitrile in a round bottom flask.1mmol, 0.3464 g of **L2F** was dissolved separately in 20 mL of acetonitrile (Fig 2). The ligand solution was added dropwise into the flask containing the metal salt solution with stirring, then refluxed for 6 h. The dark yellow precipitate was filtered off, washed with a small amount of cold acetonitrile and air-

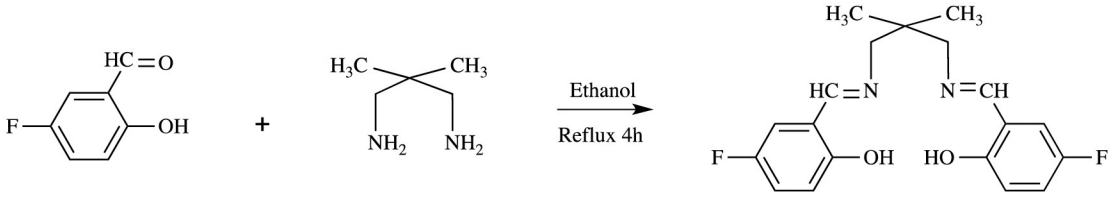

Fig 1. Synthesis of L2F.

https://doi.org/10.1371/journal.pone.0231147.g001

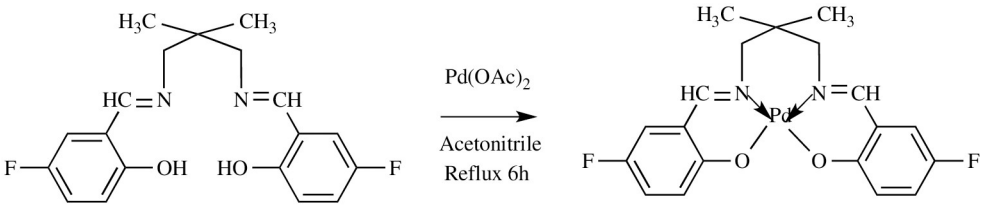

Fig 2. Synthesis of PdL2F.

https://doi.org/10.1371/journal.pone.0231147.g002

dried. The yellow single crystal of the complex was obtained upon slow evaporation of DMSO: MeOH (1:1 v/v). The synthesized compound was identified as 2,2'-((1*E*,1'*E*)-((2,2-dimethylpropane-1,3-diyl)bis-(azanylylidene))bis(methanylylidene))bis(4-fluorophenol)palladium(II), a tetradentate Schiff base complex denoted as PdL2F. Yellow solid; yield, 55.5%; m.p. 295–300 ˚C. Elemental analysis for PdL2F, analysed as $C_{19}H_{18}F_2N_2O_2Pd$ (450.78 $gmol^{-1}$); % Found (Calc.) C, 50.10 (50.63): H, 3.92 (4.03); N, 6.92 (6.21); UV-Vis bands (MeCN, nm): π-π* (C = N) 255, n-π* (C = N) 410; IR bands (KBr pellet, cm^{-1}): ν(C = N) 1616, ν(C-O) 1079, ν(C = C) 1545, ν (C-H sp^2) 3041, ν(C-H sp^3) 2960; ^{1}H NMR (500 MHz, $CDCl_3$, ppm): δ(HC = N) 7.96 (s, 1H); ^{13}C NMR (500 MHz, $CDCl_3$, ppm): δ(C = N) 164.40.

Cytotoxicity test. The HCT 116 (ATCC, CCL247) colorectal carcinoma cells were obtained from the American Type Culture Collection (ATCC), Manassas, VA, USA. The cells were maintained in Roswell Park Memorial Institute (RPMI) 1640 medium supplemented with 10% heat activated fetal bovine serum and 1% penicillin-streptomycin at 37˚C in a 5% CO_2 atmosphere. The HCT116 cells were seeded at 2,000 cells/ 200 μL onto each well of the 96-well plate and were treated with Schiff base ligand (L2F) and palladium(II) (PdL2F) (0.01–100 μg/mL) followed by incubation for 72 hours at 37˚C and 5% CO_2 overnight. DMSO (0.001–10%) and 5-FU (0.01–100 μg/mL) were also included as vehicle and positive controls, respectively. Treated cells were fixed with 10% (w/v) tricholoracetic acid (TCA) at 4 ˚C for 30 minutes. The fixed cells were washed with tap water. Each well was stained with 0.4% (w/v) SRB solution at room temperature for 10–15 minutes. The plate was rinsed with (1% v/v) acetic acid for the removal of the unbound dye and left to dry overnight. Tris base (10 mM) was added for dye solubilisation. The plate was read at 570 nm. Data obtained was used to plot the dose-response curve from which IC_{50} was determined. IC_{50} value is defined as the concentration of a test compound required to achieve half maximal inhibition [35].

Theoretical details

Geometry optimisation and frequency calculations of **L2F** Schiff base and its corresponding complex with palladium metal were performed using DFT method. Five hybrid functionals B3LYP, B3P86, CAM-B3LYP and PBE0 combined with LanL2DZ basis set were tested [36]. The true minima of the optimized structure were confirmed by the absence of imaginary frequencies. The calculated vibrational modes were scaled by a factor of 0.9679 [37]. Excited states (ES) calculations were performed using TD-DFT method. The maximum absorption bands, vertical electronic excitations and oscillator strengths (f>0 for allowed transition) were calculated using the five hybrid functions [38, 39]. The predicted magnetic isotropic shielding tensors (σ) were calculated using the standard Gauge-Independent Atomic Orbital approach (GIAO) [40], using the hybrid functional B3LYP combined with LanL2DZ basis set. The isotropic shielding values were used to calculate the isotropic chemical shifts δ with respect to the reference tetramethylsilane ($Si(CH_3)_4$). $\delta_{iso}(X) = \sigma_{TMS}(X) - \sigma_{iso}(X)$, where δ_{iso} is isotropic chemical shift and σ_{iso} isotropic shielding constant. The predicted chemical shifts were obtained

using the equation $\delta_{exp} = a\delta_{cal}+b$, where $\delta_{cal} = \delta_{iso}$. The solvation effect was considered implicitly using polarisable continuum model (PCM) [41]. In such model, the tilted substrates were embedded into a shape-adapted cavity surrounded by a dielectric continuum solvent, described by its dielectric constant (e.g., $\varepsilon_{CDCl3} = 4.7113$). The PCM has been reported to correctly model major solvent effects such as electrostatic effects of the medium, providing no specific solute-solvent interactions such as hydrogen bond interactions, dipole-dipole interactions, or induced dipole-dipole interactions [42]. For excited state calculations, the solvent effects were considered by using IEF-PCM and state-specific solvation (SS-PCM) [43, 44]. DFT calculations were performed using Gaussian09 package [45].

Results and discussion

UV-visible spectroscopy

The main experimental and predicted maximum absorption bands of **L2F** Schiff base and **PdL2F** are shown in Tables 1 and 2. The observed λ_{MAX} at 257 nm as shown in Fig 3 is attributed to π-π^* electronic transition of the C = N chromophore, and it is in accordance with the value reported by Khanmohammadi, Salehifard, & Abnosi, (2009) [46]. Theoretically, this band corresponds to an electronic transition between HOMO and LUMO orbitals. As can be seen from Table 3, this band was well reproduced with the B3LYP and B3P86 hybrid functionals in gas, IEF-PCM and SS-PCM phases (Table 1). For instance, by using B3LYP hybrid functional for **L2F**, variations of 2, 0 and 3 nm with respect to the experimental value were obtained in gas, IEF-PCM and SS-PCM phases, respectively. This band was slightly influenced by the solvatochroism effect where both models IEF-PCM and SS-PCM showed negligible shifts of the corresponding value obtained in gas phase with both B3LYP and B3P86 hybrid functional with variation less than 3 nm. The solvent effect may arise from intermolecular H-bonding or weaker van der Waal's forces between the F and O-containing Schiff base with the solvent, acetonitrile. CAM-B3LYP and PBE0 failed in the reproduction of the experimental value of the observed band at 275 nm. CAM-B3LYP and PBE0 hybrid functionals for **L2F** underestimated the experimental value with variations of 22 and 10 nm in gas phase, respectively. The complexation of the Schiff base ligand **L2F** with Pd (II) has an effect on the observed band at 257 nm with slight hypsochromic shift (blue shift) of 2 nm. Similarly, the band at 255 nm of **PdL2F** complex was well reproduced with B3P86 and B3LYP, while it is

Table 1. λ_{MAX} (nm), E_{MAX} (eV), *f* of $\pi \rightarrow \pi^*$ transitions of L2F and PdL2F calculated using B3LYP, PBE0, CAM--B3LYP and PBE0 hybrid functional in gas, IEF-PCM and SS-PCM.

	Gas			IEF-PCM			SS-PCM			Experimental	
	λ_{MAX}	E_{MAX}	*F*	λ_{MAX}	E_{MAX}	*f*	λ_{MAX}	E_{MAX}	*f*	λ_{MAX}	E_{MAX}
B3LYP											
L2F	259	4.79	0.29	257	4.82	0.48	260	4.77	0.67	257	4.82
PdL2F	259	4.78	0.20	258	4.80	0.39	261	4.75	0.60	255	4.86
B3P86											
L2F	258	4.81	0.28	256	4.84	0.47	259	4.79	0.67	257	4.82
PdL2F	256	4.84	0.16	254	4.87	0.32	257	4.83	0.48	255	4.86
CAM-B3LYP											
L2F	235	5.28	0.38	234	5.29	0.46	237	5.23	0.62	257	4.82
PdL2F	223	5.57	0.68	232	5.35	0.65	236	5.25	0.93	255	4.86
PBE0											
L2F	247	5.01	0.47	247	5.02	0.58	250	4.95	0.77	257	4.82
PdL2F	247	5.02	0.25	245	5.05	0.48	248	4.99	0.68	255	4.86

https://doi.org/10.1371/journal.pone.0231147.t001

Table 2. λ_{MAX} (nm), E_{MAX} (eV), *f* of electronic transitions of L2F (n→π*) and its complexes and PdL2F (n→d) calculated using B3LYP, PBE0, CAM-B3LYP and PBE0 hybrid functional in gas, IEF-PCM and SS-PCM.

	Gas			IEF-PCM			SS-PCM			Experimental	
	λMAX	EMAX	f	λMAX	EMAX	f	λMAX	E_{MAX}	*f*	λMAX	E_{MAX}
B3LYP											
L2F	337	3.68	0.14	327	3.80	0.18	332	3.73	0.23	327	3.79
PdL2F	366	3.38	0.08	352	3.52	0.08	356	3.48	0.13	410	3.02
B3P86											
L2F	339	3.66	0.13	331	3.75	0.18	336	3.69	0.22	327	3.79
PdL2F	362	3.43	0.08	407	3.05	0.06	411	3.02	0.12	410	3.02
CAM-B3LYP											
L2F	301	4.12	0.20	293	4.23	0.22	299	4.15	0.27	327	3.79
PdL2F	365	3.40	0.16	346	3.59	0.21	353	3.51	0.33	410	3.02
PBE0											
L2F	325	3.81	0.17	318	3.90	0.19	324	3.83	0.24	327	3.79
PdL2F	347	3.57	0.08	387	3.20	0.09	392	3.16	0.17	410	3.02

https://doi.org/10.1371/journal.pone.0231147.t002

underestimated with CAM-B3LYP and PBE0 hybrid functionals with variations of 32 and 8 nm, respectively.

The strong maximum absorption band observed at the higher wavelength of 327 nm in the UV-Vis spectrum of **L2F** is assigned to n-π* electronic transition of the imine chromophore. This band indicates that there is a transition of electrons from the non-bonding n orbital to the anti-bonding π* orbital [47, 48]. Theoretically, this band corresponds to an electronic transition between HOMO and LUMO orbitals of **L2F** Schiff base. Referring to Table 2, in the gas phase, λ_{MAX} at 327 nm was overestimated with the B3LYP and B3P86 functionals and underestimated with CAM-B3LYP and PBE0 functionals. The best reproduction for the gas phase was

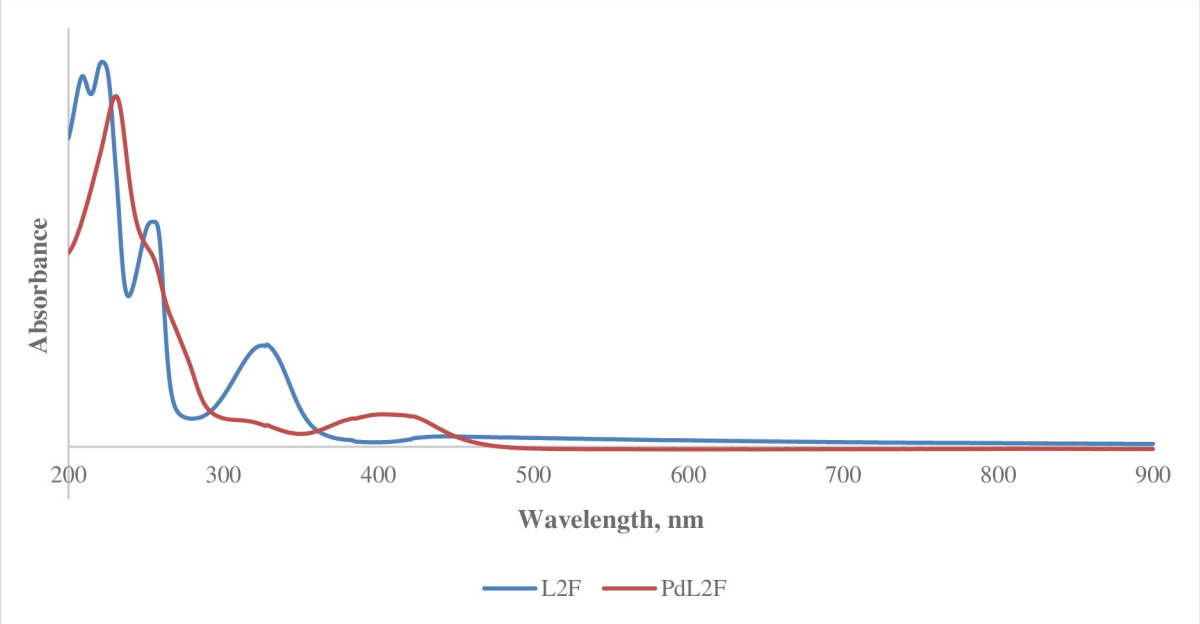

Fig 3. UV-vis spectra of L2F and PdL2Fs.

https://doi.org/10.1371/journal.pone.0231147.g003

obtained with the PBE0 hybrid functional with a variation of 2 nm with respect to the experimental value. This λ_{MAX} was seen to be strongly affected by the solvent with hypsochromic shifts (blue shift) obtained in different hybrid functionals. The exact reproduction of λ_{MAX} of **L2F** at 327 in IEF-PCM was obtained with B3LYP hybrid functional, while in SS-PCM the best reproduction was obtained with PBE0 hybrid functional with variation of 3 nm. The blue shift of λ_{MAX} at 327 nm in solvent is mainly referred to the solute-solvent interactions and to the formation of hydrogen bonding of L2F with solvent molecules. The results are in agreement with the values and trend reported by More et al., (2017) [49].

Upon complexation with Pd (II), the λ_{MAX} experienced a bathochromic (red) shift to a higher wavelength of 410 nm. This is in agreement with the weakening of the C = N when the lone pair of electrons on N is donated to the Pd (II) in a Lewis acid-base interaction. The best reproduction of this band was obtained with B3P86 in SS-PCM and IEF-PCM with variation of 1 and 3 nm with respect to the experimental value, respectively. It is worth to mention that the solute-solvent interactions induce a bathochromic shift (red shift) of the n-π^* band.

Infrared spectroscopy

The calculated, scaled and experimental main vibrational modes of **L2F** and **PdL2F** are reported in Table 3. The characteristic peak for imine, ν(C = N), is found at 1637 cm^{-1} in the spectrum of the free ligand, L2F. The best reproduction of this band was obtained with PBE0 hybrid functional with a variation of 3 cm^{-1} with respect to the observed value (Table 3). Other tested functionals namely B3LYP, B3P86 and CAM-B3LYP, reproduced the peak less accurately with variations of 31, 24 and 20 cm^{-1} with respect to the observed value, respectively. This vibration mode experienced a shift of 21 cm^{-1} to a lower frequency of 1616 cm^{-1} in the spectrum of PdL2F as can be seen in Fig 4, indicating that complexation has been established through bonding of imine nitrogen and Pd (II) center [50]. The C = N bond became weaker upon complexation as a result of the inductive effect of lone electron pair on imine nitrogen being shared with the metal centre.

The weak vibration of hydroxyl group ν(OH) of **L2F** is found at 2393 cm^{-1}. The best reproduction of this vibration mode was obtained with B3LYP functional with a variation of 44 cm^{-1}, while other tested functionals failed in its reproduction with variation higher than that. The weak peak of OH indicated the occurrence of hydrogen bonding OH···N = C occurring in intramolecular manner between –OH with imine nitrogen [51], as reported in Table 7. Noticeably, this signal disappeared in the PdL2F complex signalling that the complexation was established through deprotonation of the phenolic hydroxyl [52] prior to bonding with Pd (II) center. The shifting of ν(C-O) peak to a higher frequency by 8 cm^{-1} in PdL2F complex further supported the involvement of phenolic oxygen in complexation [53, 54].

NMR spectroscopy

The experimental and the predicted ^{1}H and ^{13}C chemical shifts of **L2F** and **PdL2F** are shown in Table 4 and Fig 5. The observed proton of OH group of **L2F** appears as singlet in the downfield region at 13.25 ppm due to the formation of intramolecular hydrogen bonding with the imine nitrogen [50]. Theoretically, this chemical shift was well reproduced in in gas and PCM phases, with variations of 0.45 and 0.25 ppm, respectively. The absence of OH peak in the spectra of PdL2F supported the infrared evidence that the coordination to metal centres was established through deprotonation of the hydroxyl groups [55]. The chemical shift for the imine proton, HC = N, was detected as a singlet in the region of 8.32 ppm for **L2F**. The predicted corresponding one in gas and PCM phases appeared at 7.9 and 8.0 ppm, respectively. The complexation of the ligand with Pd (II) shifted this peak downfield to 7.96 ppm. This shift was

Table 3. Calculated, scaled and experimental vibrational modes of L2F and its complexes PdL2F.

	L2F			PdL2F		
	Cal	Scal	Exp	Cal	Scal	Exp
ν_{O-H}						
B3LYP	2349	2274	2393	-	-	-
B3P86	2092	2025	2393	-	-	-
CAM-B3LYP	2506	2426	2393	-	-	-
PBE0	2214	2143	2393	-	-	-
ν_{C-H} (ar)						
B3LYP	3250	3146	3274	3245	3141	3225
B3P86	3269	3164	3274	3265	3160	3225
CAM-B3LYP	3277	3172	3274	3276	3171	3225
PBE0	3280	3175	3274	3276	3171	3225
$\nu_{C=N}$						
B3LYP	1661	1608	1637	1643	1590	1616
B3P86	1667	1613	1637	1662	1609	1616
CAM-B3LYP	1712	1657	1637	1695	1641	1616
PBE0	1688	1634	1637	1677	1623	1616
$\nu_{C-H(sp^2)}$						
B3LYP	3108	3008	3071	3139	3038	3041
B3P86	3133	3032	3071	3155	3054	3041
CAM-B3LYP	3138	3037	3071	3170	3068	3041
PBE0	3141	3040	3071	3251	3147	3041
$\nu_{C-H(sp^3)}$						
B3LYP	3057	2959	2956	3037	2940	2960
B3P86	3044	2946	2956	3051	2953	2960
CAM-B3LYP	3049	2951	2956	3061	2963	2960
PBE0	3059	2961	2956	3061	2963	2960

Cal = Calculated; Scal = Scaled; Exp = Experimental

https://doi.org/10.1371/journal.pone.0231147.t003

reproduced theoretically, appearing at 7.9 ppm. This supports the observation made in IR spectroscopy of the involvement of imine nitrogen in the coordination to the metal centre [56].

The experimental and predicted chemical shifts of aromatic protons of free ligands appeared as multiplets in the range of 6.78–7.19 ppm for the free ligand. This is in agreement with the chemical shifts reported by Ahmad et al., (2018) [57]. These hydrogens experience the shielding effect of diamagnetic anisotropy caused by circulating π electrons in the aromatic rings [58]. The signals of these aromatic protons were found at 6.77–7.18 ppm in the complex. The shifting in chemical shift of these protons indicates that the complexation has been established between metal ions and the ligands. Good correlations are obtained between the experimental and the predicted proton chemical shifts of **L2F** and its complex **PdL2F** with correlation coefficient coefficients of 99.64 and 99.91%, respectively.

The ^{13}C NMR chemical shift of azomethine carbon, HC = N is found at 164.74 ppm in the free ligand. The corresponding predict one appears at 164 ppm in gas phase. However, in PCM phase downfield of the signal is observed with a variation of 7.26 ppm with respect to the experimental value. The signal of C-OH is observed at 158 ppm, slightly up field with respect to HC = N signal. Characteristic peaks of aliphatic and aromatic methyl were observed at 36.30 ppm and 24.36 ppm, respectively. Aromatic carbons were detected in the range of

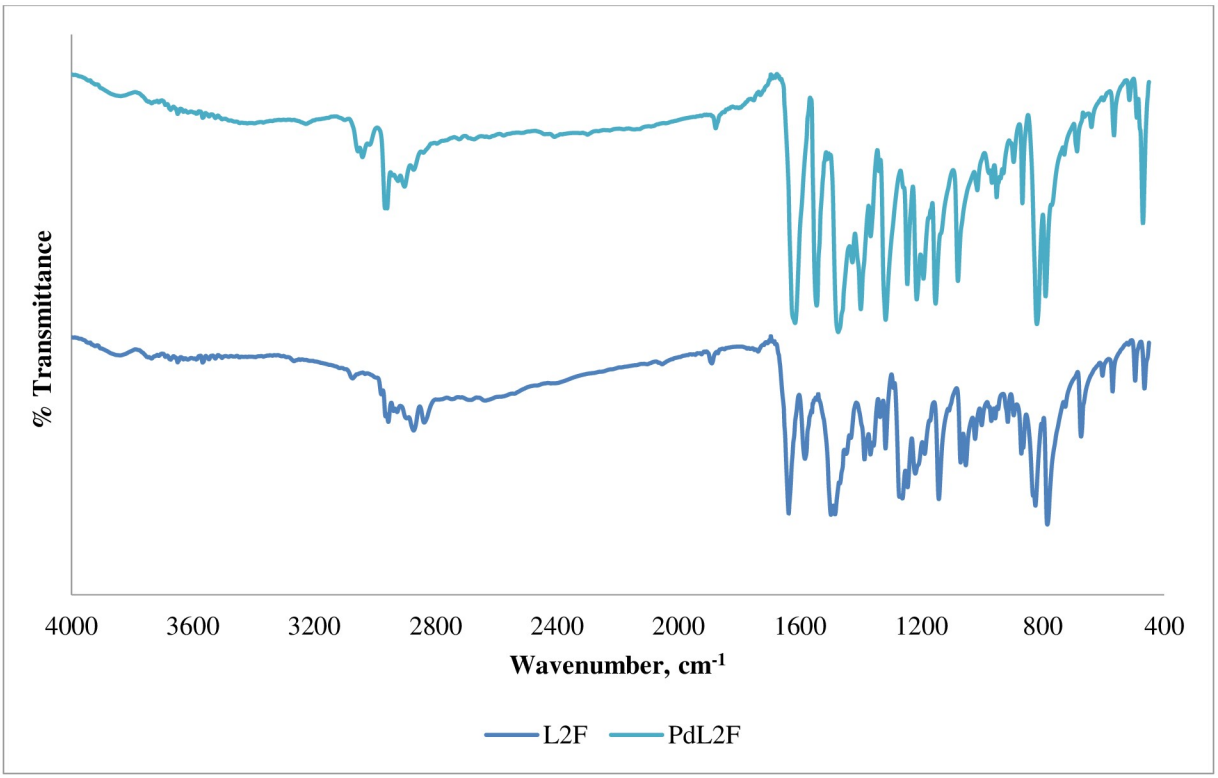

Fig 4. FTIR spectra of L2F and PdL2F.

https://doi.org/10.1371/journal.pone.0231147.g004

Table 4. Predicted and experimental ^{1}H and ^{13}C chemical shifts of L2F and its complex PdL2F.

	L2F			PdL2F		
^{1}H-NMR	**Gas**	**PCM**	**Exp.**	**Gas**	**PCM**	**Exp.**
OH	12.8	13.5	13.25			-
HC = N	7.9	8.0	8.30	7.9	7.9	7.96
Ar-H	6.8	6.9	6.91–7.35	7.0	7.0	6.76–7.20
CH_3	1.5	1.3	0.97	1.2	1.1	1.02
CH_2	3.1	3.3	3.5	3.3	3.4	3.53
^{13}C-NMR						
C (OH)	160	167	157.74	-		ND
HC = N	164	172	164.74	164	163	164.4
Ar-C	113	121	116.35–119.51	115	116	117.76–120.66
Ar-F	157	164	156.34	-		ND
CH_3	21	29	24.36	18	18	23.66
$-CH_2-$	70	77	68.2	76	76	71.02
$-C(CH_3)_2$	40	48	36.3	37	38	33.95

https://doi.org/10.1371/journal.pone.0231147.t004

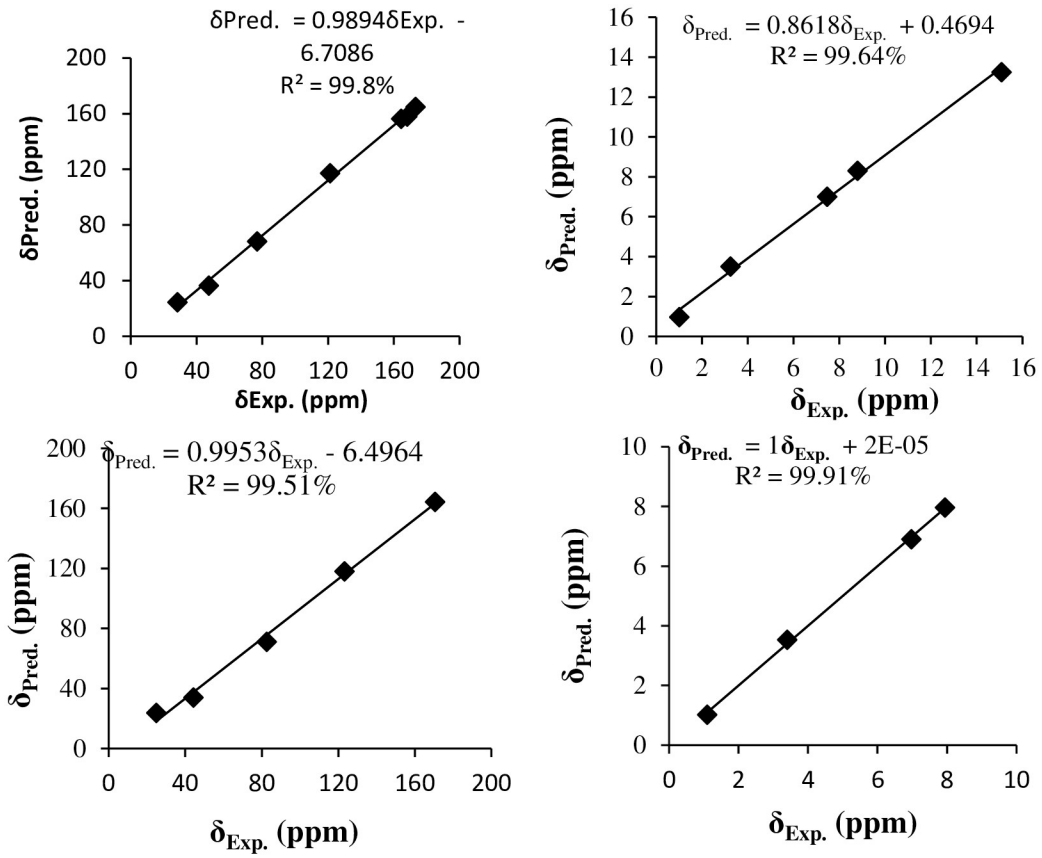

Fig 5. Correlation curves between the experimental and predicted ^{13}C NMR (right) and ^{1}H NMR (left) chemical shifts of L2F Schiff base (up) and its complex PdL2F (bottom).

https://doi.org/10.1371/journal.pone.0231147.g005

117.96–156.34 ppm. The ^{13}C NMR chemical shifts of **L2F** and **PdL2F** are well reproduced with correlation coefficients of 99.8 and 99.51%, respectively (Fig 5).

Crystal structure description

The ligand **L2F** and complex **PdL2F** crystallized in Pī and monoclinic system respectively. The crystal system and refinement parameters are given in Table 5.

Fig 6 shows the molecular structure of the ligand with the numbering scheme. The molecule consists of two 2-fluoro (2-iminoethyl) phenol groups linked by 2,2-dimethyl-1,3- dimethylenepropane moiety.

The two 2-fluoro (2-iminoethyl) phenol groups F1/O1/N1/C1-C8 and F2/O2/N1/C10-C17 are each planar with maximum deviation of 0.039(2) and 0.048(2) Å for fluorine atom (F1 and F2) respectively from their mean square planes. Both planes make dihedral angle of 42.26˚. The N1/C8/C9 and N2/C10/C9 are planar with maximum deviation of 0.008 (2) Å for atom N1 from the least square plane and the torsion angle of C9-C8-N1-C7 and C9-C10-N2-C11 are 147.68 ˚ and 138.19(19) ˚ respectively. The bond length and angles are in normal ranges (Table 6). There are two intramolecular hydrogen bonds O1-H1A. . .N1 and O2-H2A. . .N2 in the molecule (Table 7). No intermolecular hydrogen bonds were observed.

The ligand formed 1:1 complex with palladium acetate through coordination via nitrogen and phenolic oxygen atoms to form a square planar geometry (Fig 7). Both phenolic OH

Table 5. Crystallographic data and refinement parameters for L2F and PdL2F.

Compound	L2F	PdL2F
Chemical formula	$C_{19}H_{20}F_2N_2O_2$	$C_{19}H_{18}F_2N_2O_2Pd$
Molecular weight	346.37	450.75
Temperature (K)	0(2)	273(2)
Wavelength (Å)	0.71073	0.71073
Crystal system	Triclinic	monoclinic
Space group	Pī	P21/c
Unit cell dimensions (Å)	a = 6.1334(5), b = 9.2490(7), c = 16.3270(13)	a = 11.111(2), b = 13.701(3), c = 12.196(2)
Angles(˚)	α = 102.110(2), β = 96.032(2), γ = 103.520(2)	β = 105.069(6)
Volume ($Å^3$)	868.84(12)	1792.8(6)
Z	2	4
Absorption coefficient (mm^{-1})	0.101	1.313
F(0 0 0)	364	904
Crystal size	0.50 × 0.29 × 0.19 mm	0.27 × 0.20 × 0.08 mm
No. of reflections collected	25298	51046
No. of independent reflections	4327	4443
***θ* range (˚)**	2.930–28.370	2.973–28.353
Index ranges	-7< = h< = 8	-14< = h< = 14
	-12< = k< = 12	-18< = k< = 18
	-21< = l< = 21	-16< = l< = 16
Goodness-of-fit on F2	1.052	1.106
***R* indices**	*R1* = 0.0626, *wR2* = 0.1294	*R*1 = 0.0646, *wR2* = 0.1229
***R* indices (all data)**	*R1* = 0.1003, *wR2* = 0.1500	*R*1 = 0.0925, *wR2* = 0.1428
CCDC no.	1855625	1890435

https://doi.org/10.1371/journal.pone.0231147.t005

groups were deprotonated. The nitrogen atoms are at *trans* position to oxygen atoms. The *trans* N-Pd1-O angles are about 172˚ and the cis angles about the central Pd1 atom between 80.42 (17) and 94.79 (19)˚ indicate a distorted square planar geometry.

The coordination also creates three 6-membered rings, Pd1-N1-C7-C8-C5-O1, Pd1-N2-C11-C12-C17-O2 and Pd1-N1-C8-C9-C10-N2. The first two rings are essentially planar with maximum deviation of 0.079 (4) Å for O2 atom from the least square plane. However, the Pd1-N1-C8-C9-C10-N2 ring adopts half chair conformation with C9 atom deviated by 0.404(6) Å for C10 atom from the least square plane (Fig 7).

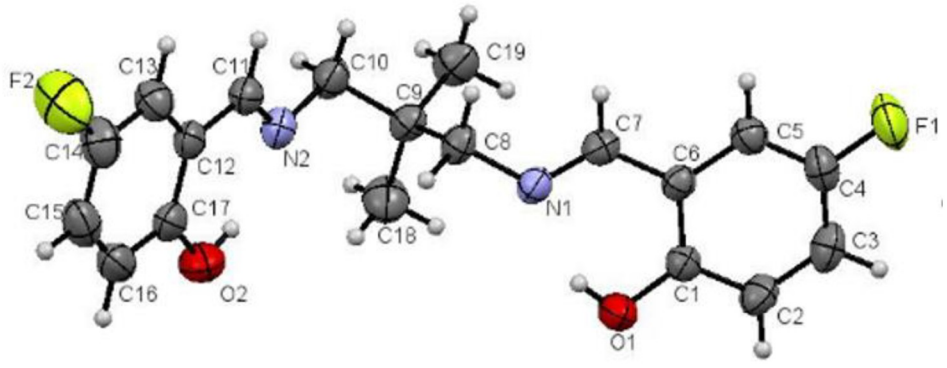

Fig 6. Molecular structure of ligand drawn at 50% probability ellipsoids.

https://doi.org/10.1371/journal.pone.0231147.g006

Table 6. Some important bond lengths (Å) and angles (˚) of L2F and PdL2F.

Bond length/angle	L2F	PdL2F
O1-C1	1.348(2)	1.306(7)
O2-C17	1.349(3)	1.308(7)
N1-C7	1.270(2)	1.280(8)
N1-C8	1.458(2)	1.480(7)
N2-C11	1.270(3)	1.297(8)
N2-C10	1.456(3)	1.467(7)
Pd1-O1	-	1.994(4)
Pd1-N2	-	1.997(5)
Pd1-O2	-	2.000(4)
Pd1-N1	-	2.013(4)
O1-Pd1-N2	-	172.85(18)
O1-Pd1-O2	-	80.42(17)
N2-Pd1-O2	-	92.49(18)
O1-Pd1-N1	-	92.33(18)
N2-Pd1-N1	-	94.79(19)
O2-Pd1-N1	-	172.33(18)
C8-C9-C10-N2	-	-73.8(7)
C19-C9-C10-N2	-	170.5(5)
C18-C9-C10-N2	-	50.4(7)

https://doi.org/10.1371/journal.pone.0231147.t006

The O1-C1 and O2-C17 bond lengths in the complex are significantly shorter than that in the ligand as the result of the deprotonation of the phenolic groups. On the other hand, the N1-C7 and N2-C11 bond lengths are slightly longer than that in the ligand. Other bond lengths and angles are in normal ranges and comparable with those reported by Ahmad et al., (2017) [59].

In the crystal structure the complex is stabilized by C5-H5A. . .O1 intermolecular hydrogen bonds (symmetry code as in Table 7) to a zig-zag one dimensional chain along the c axis (Fig 8).

Biological activity screening

L2F and **PdL2F** were screened for their anticancer properties against HCT116. As depicted in Table 8, **PdL2F** showed a better potency against the cancer cell with IC_{50} of 4.1 μg/mL while **L2F** could be considered less active as anticancer agent with 90.00 μg/mL. Located in the same group as platinum, as well as being a soft metal with an abundance of *d* electrons, palladium is expected to interact with the DNA backbone that is rich with N, a soft donor atom. The excellent performance of the complex may also be caused by its square planar geometry which

Table 7. Hydrogen bonds in the ligand L2F and PdL2F complex.

D - -H ..A	D - -H (Å)	H ..A (Å)	D - -A (Å)	D - -H ..A (˚)
		L2F		
O1 - -H1B ..N1	0.83(2)	1.86(3)	2.619(2)	152(3)
O2 - -H2B ..N2	0.82(3)	1.84(4)	2.599(3)	153(3)
		PdL2F		
C5 - -H5A ..O1	0.93	2.46	3.376(8)	169

(symmetry codes; i = x,1/2-y,1/2+z)

https://doi.org/10.1371/journal.pone.0231147.t007

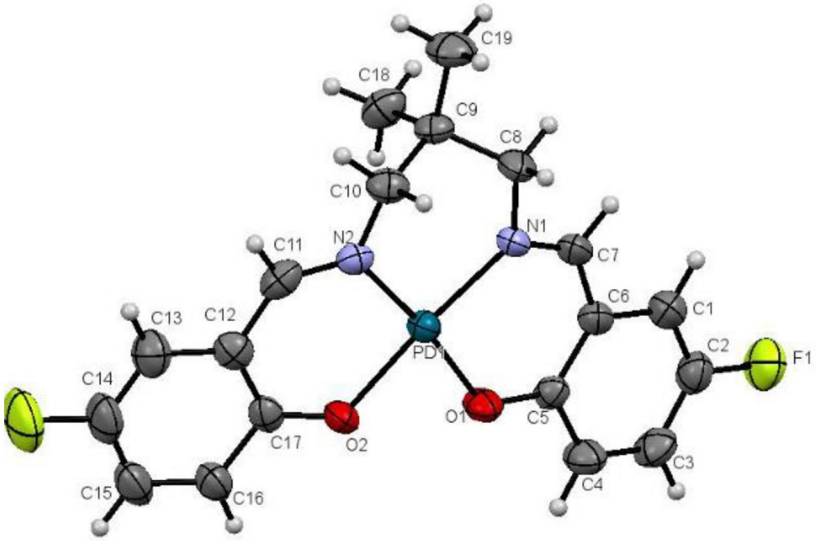

Fig 7. Molecular structure of PdL2F complex drawn at 50% probability ellipsoids.

https://doi.org/10.1371/journal.pone.0231147.g007

allowed them to stack in the structure of the DNA [60]. The structure helped palladium (II) complex kinking the pharmacological target, DNA, more effectively through a mechanism called intercalation [61]. Intercalation has been proven to stabilize, lengthen, stiffen, and at certain extent unwinds the DNA double helix. Intercalators can fit between two base pairs, opening a space between its base pairs by unwinding [62].

Conclusion

2,2'-((1E,1'E)-((2,2-dimethylpropane-1,3-diyl)-bis(azanylylidene))bis(methanylylidene))bis (4-fluorophenol), a tetradentate Schiff base named **L2F** and its complex **PdL2F**, were successfully synthesised. The molecular structures of the synthesised compounds were confirmed by spectroscopic and X-ray techniques. Anticancer activity of **PdLF** was better than its parent ligand against HCT1116 with $1C_{50}$ of 4.1 μg/mL.

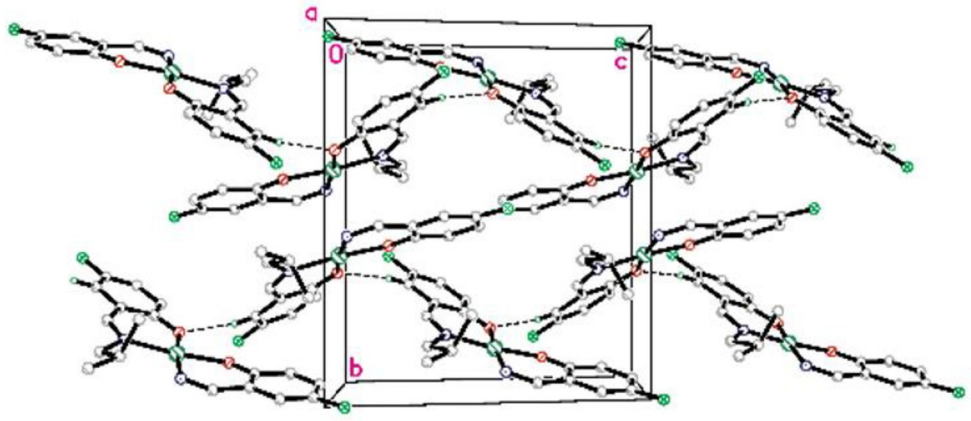

Fig 8. Molecular packing of PdL2F complex viewed down a axis. The non-hydrogenbonded hydrogen atoms are omitted for clarity.

https://doi.org/10.1371/journal.pone.0231147.g008

Table 8. The anticancer activity of L2F and its PdL2F complex against HCT116.

Compound	IC_{50}, μg/mL
L2F	90.00 (less active)
PdL2F	4.1 (active)
Positive control (5-FU)	1.70
Vehicle Control (DMSO)*	1.09

https://doi.org/10.1371/journal.pone.0231147.t008

Supporting information

S1 Fig. ^{1}H NMR spectra of L2F and PdL2F.
(DOCX)

S2 Fig. ^{13}C NMR spectra of L2F.
(DOCX)

S1 Table. Crystallographic information of L2F.
(CIF)

S2 Table. Crystallographic information L2F.
(CIF)

Acknowledgments

The authors would like to thank Coordination Chemistry Laboratory, Atta-ur-Rahman Institute for Natural Product Discovery (AuRIns), Collaborative Drug Discovery Research (CDDR) Group and Universiti Teknologi MARA (UiTM) for all the facilities used to conduct this research.

Author Contributions

Conceptualization: Nizam Ahmad.

Data curation: Nizam Ahmad, El Hassane Anouar, Amalina Mohd Tajuddin, Kalavathy Ramasamy, Bohari M. Yamin, Hadariah Bahron.

Investigation: Kalavathy Ramasamy.

Methodology: Amalina Mohd Tajuddin, Kalavathy Ramasamy.

Supervision: Amalina Mohd Tajuddin, Hadariah Bahron.

Writing – original draft: Nizam Ahmad, El Hassane Anouar, Bohari M. Yamin, Hadariah Bahron.

Writing – review & editing: Nizam Ahmad, El Hassane Anouar, Bohari M. Yamin, Hadariah Bahron.

References

1. Tidwell T. T. Hugo (Ugo) Schiff, Schiff Bases, and a century of β-Lactam synthesis. Angewandte Chemie. 2008: 1016–1020. https://doi.org/10.1002/anie.200702965 PMID: 18022986
2. Gupta K. C., & Sutar A. K. Catalytic activities of Schiff base transition metal complexes. Coordination Chemistry Reviews. 2008; 252: 1420–1450.
3. Baleizao C., & Garcia H. Chiral salen complexes: an overview to recoverable and reusable homogeneous and heterogeneous catalysts. Chem. Rev., 2006; 106: 3987–4043. https://doi.org/10.1021/cr050973n PMID: 16967927

4. Keypour H., Salehzadeh S., & Parish R. V. Synthesis of two potentially heptadentate (N4O3) Schiff-base ligands derived from condensation of tris(3-aminopropyl)-amine and salicylaldehyde or 4-hydroxysalicylaldehyde. Nickel(II) and copper(II) complexes of the former ligand. Molecules. 2002; 7(2):140–144.
5. Abdel-Rahman L. H., Abu-Dief A. M., El-Khatib R. M., & Abdel-Fatah S. M. Some new nano-sized Fe (II), Cd(II) and Zn(II) Schiff base complexes as precursor for metal oxides: Sonochemical synthesis, characterization, DNA interaction, in vitro antimicrobial and anticancer activities. Bioorganic Chemistry. 2016; 69: 140–152. https://doi.org/10.1016/j.bioorg.2016.10.009 PMID: 27816797
6. Alim A., Zahan K. E., Haque M., & Tarafder M. Synthesis and characterization of some metal complexes of Cu(II), Ni(II), Zn(II), Cd(II), Sn(II), Co(II), Sb(III) and Fe(III) containing bidentate Schiff base of Smdtc. Science Journal of Chemistry. 2015; 3(3): 35–39.
7. Tarafder M., Kasbollah A., Saravanan N., Crouse K.A., Ali A.M., S-methyldithiocarbazate and its Schiff bases: evaluation of bondings and biological properties. Journal of Biochemistry, Molecular Biology, and Biophysics: JBMBB: the official journal of the Federation of Asian and Oceanian Biochemists and Molecular Biologists (FAOBMB). 2002; 6(2): 85.
8. Chohan Z.H., Arif M., Shafiq Z., Yaqub M., Supuran C.T., In vitro antibacterial, antifungal & cytotoxic activity of some isonicotinoylhydrazide Schiff's bases and their cobalt(II), copper (II), nickel (II) and zinc (II) complexes, Journal of Enzyme Inhibition and Medicinal Chemistry. 2006; 21(1): 95–103. https://doi.org/10.1080/14756360500456806 PMID: 16570512
9. Guo Z., Xing R., Liu S., Zhong Z., Ji X., Wang L., et al, Antifungal properties of Schiff bases of chitosan, N-substituted chitosan and quaternized chitosan. Carbohydrate Research. 2007; 342(10): 1329–1332. https://doi.org/10.1016/j.carres.2007.04.006 PMID: 17485075
10. Taha M., Baharudin M.S., Ismail N.H., Khan K.M., Jaafar F.M., Siddiqui S., et al. Synthesis of 2-methoxybenzoylhydrazone and evaluation of their antileishmanial activity. Bioorganic & Medicinal Chemistry Letters. 2013; 23(11): 3463–3466
11. Anouar E.H., Raweh S., Bayach I., Taha M., Baharudin M.S., Di Meo F., et al. Trouillas, Antioxidant properties of phenolic Schiff bases: structure–activity relationship and mechanism of action. Journal of Computer-aided Molecular Design. 2013; 27(11): 951–964. https://doi.org/10.1007/s10822-013-9692-0 PMID: 24243063
12. Ebrahimipour S.Y., Abaszadeh M., Castro J., Seifi M., Synthesis, X-ray crystal structure, DFT calculation and catalytic activity of two new oxido-vanadium(V) complexes containing ONO tridentate Schiff bases. Polyhedron. 2014; 79: 138–150.
13. Tajuddin A.M., Ramasamy K., Yamin B.M., Alharthi A.I., Bahron H., DFT analysis and bioactivity of 2-((E)-(4-methoxybenzylimino)methyl) phenol and its Ni(II) and Pd(II) complexes. Arabian Journal of Chemistry. 2017; 10(6): 769–780.
14. Gauss J., Calculation of NMR chemical shifts at second-order many-body perturbation theory using gauge-including atomic orbitals. Chemical Physics Letters. 1992; 191(6): 614–620.
15. Gauss J. Effects of electron correlation in the calculation of nuclear magnetic resonance chemical shifts, J. Chem. Phys. 1993; 99(5): 3629–43.
16. Gauss J. Accurate calculation of NMR chemical shifts, Ber. Bunsen-Ges. 1995; 99(8):1001–1008.
17. Bak K., Hansen A., Ruud K., Helgaker T., Olsen J., Jørgensen P. Ab initio calculation of electronic circular dichroism fortrans-cyclooctene using London atomic orbitals, Theoret. Chim. Acta. 1995: 90(5–6): 441–458.
18. Bauernschmitt R., Ahlrichs R. Treatment of electronic excitations within the adiabatic approximation of time dependent density functional theory. Chemical Physics Letters. (1996); 256(4–5): 454–464.
19. Casida M.E., Jamorski C., Casida K.C., Salahub D.R. Molecular excitation energies to high-lying bound states from time-dependent density-functional response theory: characterization and correction of the time-dependent local density approximation ionization threshold. The Journal of Chemical Physics. 1998; 108(11): 4439–4449.
20. Mendoza-Wilson A.M., Glossman-Mitnik D. CHIH-DFT study of the electronic properties and chemical reactivity of quercetin. Journal of Molecular Structure. THEOCHEM. 2005; 716(1–3): 67–72.
21. Vázquez-Vuelvas O.F., Hernández-Madrigal J.V., Gaviño R., Tlenkopatchev M.A., Morales-Morales D., Germán-Acacio J.M., et al. X-ray, DFT, FTIR and NMR structural study of 2,3-dihydro-2-(R-phenylacylidene)-1,3,3-trimethyl-1H-indole. Journal of Molecular Structure. 2011; 987(1–3):106–118.
22. Jacquemin D., Perpete E.A., Scuseria G.E., Ciofini I., Adamo C. TD-DFT performance for the visible absorption spectra of organic dyes: conventional versus long-range hybrids. Journal of Chemical Theory and Computation. 2007; 4(1): 123–135.
23. Jacquemin D., Preat J., Charlot M., Wathelet V., Andre J.-M., Perpete E.A. Theoretical investigation of substituted anthraquinone dyes. The Journal of Chemical Physics. 2004; 121(4): 1736–1743. https://doi.org/10.1063/1.1764497 PMID: 15260723

24. Jacquemin D., Preat J., Wathelet V., Fontaine M., Perpète E.A. Thioindigo dyes: highly accurate visible spectra with TD-DFT. Journal of the American Chemical Society. 2006; 128(6): 2072–2083. https://doi.org/10.1021/ja056676h PMID: 16464110

25. Jacquemin D., Wathelet V., Preat J., Perpète E.A. Ab initio tools for the accurate prediction of the visible spectra of anthraquinones. Spectrochimica Acta Part A: Molecular and Biomolecular Spectroscopy. 2007; 67(2): 334–341. https://doi.org/10.1016/j.saa.2006.07.023 PMID: 16959534

26. Woodford J.N. A DFT investigation of anthocyanidins. Chemical Physics Letters. 2005; 410(4–6): 182–187.

27. Anouar E.H., Gierschner J., Duroux J.-L., Trouillas P., UV/Visible spectra of natural polyphenols: A time-dependent density functional theory study. Food Chemistry. 2012; 131(1):79–89.

28. Lumpi D., Horkel E., Plasser F., Lischka H., Fröhlich J. Synthesis, spectroscopy, and computational analysis of photoluminescent bis(aminophenyl)-substituted thiophene derivatives. ChemPhysChem. 2013; 14(5): 1016–1024. https://doi.org/10.1002/cphc.201201006 PMID: 23440980

29. Quartarolo A.D., Russo N. A computational study (TDDFT and RICC2) of the electronic spectra of pyranoanthocyanins in the gas phase and solution. Journal of Chemical Theory and Computation. 2011; 7 (4): 1073–1081. https://doi.org/10.1021/ct2000974 PMID: 26606355

30. Ramos Sousa F.F., Quartarolo A.D., Sicilia E., Russo N. A time-dependent density functional study of a non-aromatic [1.1. 1.1. 1]-pentaphyrin and its lutetium complex. The Journal of Physical Chemistry B. 2012; 116(35): 10816–10823. https://doi.org/10.1021/jp3068359 PMID: 22876744

31. Wolinski K., Hinton J.F., Pulay P. Efficient implementation of the gauge-independent atomic orbital method for NMR chemical shift calculations. Journal of the American Chemical Society. 1990; 112(23): 8251–8260.

32. Cheeseman J.R., Trucks G.W., Keith T.A., Frisch M.J. A comparison of models for calculating nuclear magnetic resonance shielding tensors. The Journal of Chemical Physics. 1996; 104: 5497.

33. Data. Germany: University of Gottingen; 1996.

34. Sheldrick GM. SHELXTL V5.1, Software Reference Manual. Madison, WI, USA: Brukel AXS Inc.; 1997.

35. Rohilla P., Deep A., Kamra M., Narasimhan B., Ramasamy K., Mani V., . . . et al. Antimicrobial and Anticancer Evaluation of N′- (Substituted Benzylidene)-2-(Benzo[d]oxazol-3(2H) -yl) acetohydrazide Derivatives. Drug Research. 2014; 13, 1–5.

36. Becke A.D. Density-functional thermochemistry. III. The role of exact exchange. Journal of Chemical Physics. 1993; 98(7): 5648–52.

37. Andersson M., Uvdal P. New scale factors for harmonic vibrational frequencies using the B3LYP density functional method with the triple-ζ basis set 6–311+ G (d, p). The Journal of Physical Chemistry A. 2005; 109(12): 2937–2941. https://doi.org/10.1021/jp045733a PMID: 16833612

38. Furche F., Ahlrichs R. Adiabatic time-dependent density functional methods for excite d state properties. The Journal of Chemical Physics. 2002; 117: 7433.

39. Scalmani G., Frisch M.J., Mennucci B., Tomasi J., Cammi R., Barone V. Geometries and properties of excited states in the gas phase and in solution: theory and application of a time-dependent density functional theory polarizable continuum model. The Journal of Chemical Physics. 2006; 124: 094107.

40. Gauss J. Effects of electron correlation in the calculation of nuclear magnetic resonance chemical shifts. J. Chem. Phys. 1993; 99: 3629–43.

41. Tomasi J., Mennucci B., Cammi R. Quantum mechanical continuum solvation models. Chem. Rev. 2005; 105(8): 2999–3093. https://doi.org/10.1021/cr9904009 PMID: 16092826

42. Jacquemin D., Wathelet V., Perpete E.A., Adamo C. Extensive TD-DFT benchmark: singlet-excited states of organic molecules. Journal of Chemical Theory and Computation. 2009; 5(9): 2420–2435. https://doi.org/10.1021/ct900298e PMID: 26616623

43. Improta R., Barone V., Scalmani G., Frisch M.J. A state-specific polarizable continuum model time dependent density functional theory method for excited state calculations in solution. The Journal of Chemical Physics. 2006; 125: 054103. https://doi.org/10.1063/1.2222364 PMID: 16942199

44. Improta R., Scalmani G., Frisch M.J., Barone V. Toward effective and reliable fluorescence energies in solution by a new state specific polarizable continuum model time dependent density functional theory approach. The Journal of Chemical Physics. 2007; 127: 074504. https://doi.org/10.1063/1.2757168 PMID: 17718617

45. G.W.T. M. J. Frisch, H. B. Schlegel, G. E. Scuseria, M. A. Robb, J. R. Cheeseman, G. Scalmani, eet al. Gaussian 09, Revision A.02, 2009.

46. Khanmohammadi H., Salehifard M., & Abnosi M. H. Synthesis, characterization, biological and thermal studies of Cu(II) complexes of salen and tetrahedrosalen ligands. Journal of the Iranian Chemical Society. 2009; 6(2): 300–309.

47. Bosnich B. An interpretation of the circular dichroism and electronic spectra of salicylaldimine complexes of square-coplanar diamagnetic nickel(II). Journal of the American Chemical Society. 1968; 90 (3): 627–632.

48. Senol C., Hayvali Z., Dal H., & Hokelek T. Syntheses, characterizations and structures of NO donor Schiff base ligands and nickel(II) and copper(II) complexes. Journal of Molecular Structure. 2011; 997: 53–59.

49. More M. S., Pawal S. B., Lolage S. R., & Chavan S. S. Syntheses, structural characterization, luminescence and optical studies of Ni(II) and Zn(II) complexes containing salophen ligand. Journal of Molecular Structure. 2017; 1128, 419–427.

50. Nair M. S., Arish D., & Johnson J. Synthesis, characterization and biological studies on some metal complexes with Schiff base ligand containing pyrazolone moiety. Journal of Saudi Chemical Society. 2016; 20: S591–S598.

51. Aranha P. E., Santos M. P., Romera S., & Dockal E. R. (2006). Synthesis, characterization, and spectroscopic studies of tetradentate Schiff base chromium (III) complexes. Polyhedron. 2006; 26(7): 1373–1382.

52. Raman N., Kulandaisamy A., Thangaraja C., Manisankar P., Viswanathan S., & Vedhi C. Synthesis, structural characterisation and electrochemical and antibacterial studies of Schiff base copper complexes. Transition Metal Chemistry. 2004; 29(2): 129–135.

53. Hille A., Ott I., Kitanovic A., Kitanovic I., Alborzinia H., Lederer E., . . . et al. [N,N′-Bis(salicylidene)-1,2-phenylenediamine]metal complexes with cell death promoting properties. Journal of Biological Inorganic Chemistry. 2009; 14(5), 711–725. https://doi.org/10.1007/s00775-009-0485-9 PMID: 19259708

54. Kolawole G. A., & Patel K. S. The stereochemistry of oxovanadium(IV) complexes derived from salicylaldehyde and polymethylenediamines. Journal of the Chemical Society, Dalton Transactions. 1981; 6: 1241–1444.

55. Raman N., Pitchaikani Raja Y., & Kulandaisamy A. Synthesis and characterisation of Cu(II), Ni(II), Mn (II), Zn(II) and VO(II) Schiff base complexes derived from o-phenylenediamine and acetoacetanilide. Chem. Sci. 2001; 113(3): 183–189.

56. Maity D., Drew M. G.., Godsell J. F., Roy S., & Mukhopadhyay G. Synthesis and characterization of Cu (II) complexes of tetradentate and tridentate symmetrical Schiff base ligands. Transition Metal Chemistry. 2010; 35: 197–204.

57. Ahmad S. N., Bahron H., & Tajuddin A. M. Tetradentate palladium(II) salophen complexes: synthesis, characterization and catalytic activities in copper-free Sonogashira coupling reaction. International Journal of Engineering & Technology. 2018; 7(3.11): 15–19.

58. M.Lampman, G., L.Pavia, D., S.Kriz, G., & R.Vyvyan, J. Spectroscopy. 4th ed. 2010

59. Ahmad S. N., Bahron H., Tajuddin A. M., & Yusof M. S. M. Crystal structure of 2,2′-(((2,2-Dimethylpropane-1,3-diyl)bis(azanylylidene))-bis(methanylylidene))bis(4-methoxyphenol)palladium(II). X-Ray Structure Analysis Online. 2017; 33: 73–74.

60. Arola-arnal A., Benet-buchholz J., & Neidle S. Effects of metal coordination geometry on stabilization of human telomeric quadruplex DNA by square-planar and square-pyramidal metal complexes. Inorganic Chemistry. 2008; 47(24): 11910–11919. https://doi.org/10.1021/ic8016547 PMID: 19053336

61. Liu H.-K., & Sadler P. J. Metal Complexes as DNA Intercalators. Accounts of Chemical Research. 2011; 44(5): 349–359. https://doi.org/10.1021/ar100140e PMID: 21446672

62. Sirajuddin M., & Ali S. Drug—DNA interactions and their study by UV–Visible, fluorescence spectroscopies and cyclic voltametry spectroscopies and cyclic voltametry. Journal of Photochemistry and Photobiology A: Chemistry. 2013; 124: 1–19